INTERNATIONAL SOCIETY FOR
SOIL MECHANICS AND
GEOTECHNICAL ENGINEERING

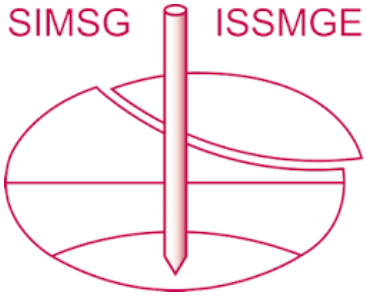

This paper was downloaded from the Online Library of the International Society for Soil Mechanics and Geotechnical Engineering (ISSMGE). The library is available here:

https://www.issmge.org/publications/online-library

This is an open-access database that archives thousands of papers published under the Auspices of the ISSMGE and maintained by the Innovation and Development Committee of ISSMGE.

5ICEGE
5th International Conference on Earthquake Geotechnical Engineering
January 2011, 10-13 | Santiago, Chile
Paper No. ESMVY

EFFECTS OF SEISMIC MOTION CHARACTERISTICS ON CYCLIC MOBILITY AND LIQUEFACTION

Antonios Vytiniotis [1], Andrew J. Whittle [2], Eduardo Kausel[2]

ABSTRACT

This paper describes numerical simulations of the response of a loose granular, waterfront embankment fill due to a suite of 62 earthquake ground motions. The analyses use the OpenSees finite element program and simulate the non-linear coupled ground deformation and transient pore pressure response using an advanced elasto-plastic effective stress soil model proposed by Dafalias & Manzari (2004). This model is able to represent realistically the laboratory measurements of pore pressure development during undrained cyclic shearing of Toyoura sand together with transitions to cyclic mobility and liquefaction phenomena. The free field responses of the 2D embankment section are performed using effective force inputs and viscous boundary conditions. The results relate the permanent embankment deformations to the peak ground accelerations, Arias intensity, directionality, and other characteristics of the measured rock outcrop motions that would be expected to cause liquefaction. It is shown that excess pore pressure development relates very well with average slope damage. It is shown that directionality of the earthquake motion does not affect in most cases observed damage, and a measure is also proposed in order to identify motions for which directionality could be important. The numerical simulations form part of a larger study on the performance and mitigation of seismic damage for pile-supported wharf structures.

Keywords: seismic motion characteristics, seismic slope stability, liquefaction

INTRODUCTION

Seismic slope stability is a very important design problem that requires sound evaluation. Newmark sliding block analysis (Newmark, 1965) in various implementations has been the most commonly used tool to investigate the seismic slope stability of slopes. More simplified analyses derived from Newmark sliding block analysis such as the Makdisi-Seed approach (Makdisi F, 1978) are also used to provide approximate seismic stability estimations. More elaborate solutions to evaluate damage in seismically excited slopes have been devised by many people such as Jibson (1994) or Bray and Travasarou (2007) but most of them seem to be formulated under very particular conditions. These more elaborate analytical solutions are most effective on dry slopes and do not always offer better performance in all cases.

The simplest form of Newmark sliding block analyses assume a constant yield acceleration on the slope thus predicting no slope damage in earthquakes with lots of cycles and acceleration less that the yield acceleration. More advanced stick-slip deformable sliding models such as the one used by Rathje and Bray (2000) can produce more accurate results but still do not incorporate all the complexities of the

[1] PhD candidate, Department of Civil and Environmental Engineering, Massachusetts Institute of Technology, e-mail: avytin@mit.edu

[2] Professor, Department of Civil and Environmental Engineering, Massachusetts Institute of Technology.

mechanical behavior of partially-draining saturated sand. More specifically, undrained soil behavior predicts that that many cycles of small shearing can lead to liquefaction and, thus, great damage, which is a phenomenon hard to capture with these analytical solutions.

A more elaborate approach is utilized in this study. A series of 62 plane-strain dynamic coupled pore-pressure displacement seismic slope stability finite element analyses is performed. The analyses represent realistically the free field boundary conditions, material behavior, and drainage conditions. These analyses are used to examine various aspects of the seismic slope stability problem; how is damage related to seismic motion characteristics, to what extent does the dilative and contractive behavior of sand affect the results, how does directionality of the ground motion affect design, and how do slope failure modes affect in-situ piles?

NUMERICAL MODEL

The numerical model was built in the OpenSees finite element software framework (Mazzoni, McKenna, & Fenves, 2005), using GiD as a pre- and post-processor. The OpenSees framework has been validated against simple analytical solutions to verify that it can correctly solve the necessary dynamic coupled pore pressure displacement PDE's (Vytiniotis, 2009).

Model Geometry

The geometry of the problem to be modeled is presented in Figure 1. The typical slope comprises a hydraulic fill overlaying a stiff clay layer. Piles are embedded in the slope supporting a wharf-deck structure. During an earthquake it is important to evaluate the damage caused in the piles, in the pile-wharf connections, and in the cranes sitting on top of the wharf. In order to evaluate damage a two-step procedure is used: The first task is simulating the free-field response of the soil (i.e. the response of the earth structure without any structures). The second part uses the predicted displacements and pore-pressure time histories as inputs to macroelements connected to the piles and superstructure. The macroelements are able to model realistically soil-pile interaction in saturated granular soils (Varun & Assimaki, 2008). This part of the research deals only with the simulation of the free field dynamic response of the soil.

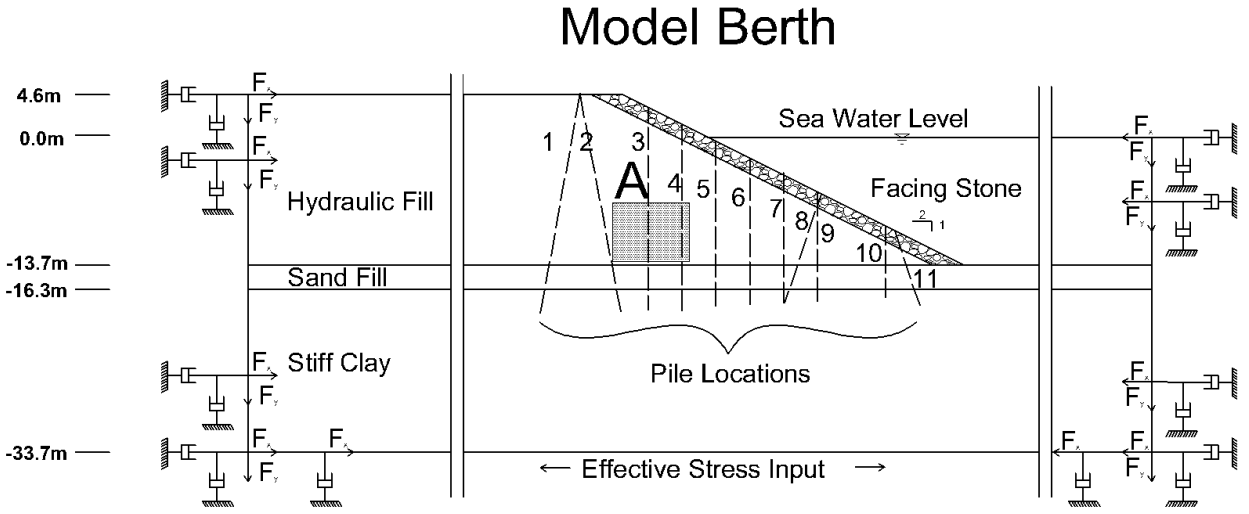

Figure 1 Modeled geometry; region A defines a region used subsequently in the averaging of excess pore pressures to define excess pore pressure vs damage correlations

Boundary Conditions
Two types of mechanical boundary conditions are of great importance in this numerical model. At first, the analysis should include the inertial effects of the sea water. Since the waves expected to be created inside the sea are not large, a reasonable approximation is to model the sea as an elastic layer with very small elastic stiffness and appropriate bulk modulus so that the p-wave velocity is matched with the p-wave-velocity of water. This approach has been found to be successful (Zienkiewicz & Bettess, 1978) if one manages to use it without introducing numerical inefficiencies.

Secondly, the analysis should include efficient absorbing boundary conditions on the bottom and on the sides to avoid wave energy getting trapped inside the model. As shown in Figure 2, effective force input and viscous dampers were used to accurately simulate the boundary conditions. The recorded ground motion is deconvolved to the level of the bottom of the grid. Then the acceleration time history is integrated to velocities, and then it is applied as effective force input on the bottom according to:

$$F = C \cdot v \cdot A \quad (1)$$

where F is the force applied, C is the viscous damping coefficient used on the bottom nodes, and A is the area on which the force is applied.

On the sides of the model a different approach is needed. Far from the slope the ground will be sheared due to vertical propagation of the shear waves and will behave like free-field soil columns. These boundaries are simulated using separate one-dimensional analysis at each lateral boundary, and record the vertical forces and the horizontal force components. These forces are applied as lateral boundaries in the 2-D slope model (Assimaki, 2004). An alternate approach would be to apply directly the ground motions recorded in the one-dimensional analyses along the sides. However, the latter approach would lead to artificial reflections.

Finally, all around the external boundaries of the model are connected with viscous boundaries applied on both the normal and tangent direction of the borders, with viscous damping, C:

$$C = v_s \cdot A \quad (2)$$

where v_s is the shear wave velocity of the soil at its current state.

Equivalent elastic properties change dramatically during cyclic mobility events, thus damping of the viscous boundaries should not remain the same in order to absorb fully waves arriving at the boundaries. In this case, energy dissipation in actual soils will smooth out any spurious reflections.

It was assumed that the water level remains constant during cyclic loading. The slope immersed in the sea acts also as a free-draining boundary.

Ground Motions
The ground motions used as input are typical of firm-site conditions in coastal California. Fifty-five ground motions were selected from the database used to develop the Next-Generation Attenuation of Ground Motions (NGA) project (Chiou et al. 2008) with minimum moment magnitude M=5.5, closest distance to rupture, 0-60km, strike-slip, reverse, or reverse-oblique, C site class, and minimum usable frequency of less than 0.5Hz. Seven ground motions are produced from the M=7.8 ShakeOut simulation on the southern San Andreas Fault. The properties of the most intense motions are summarized in Table 1.

Note that these data differ from the published characteristics for these specific motions because only the x-components of the recorded motions are considered.

Table 1 Characteristics of most intense ground motions

ID	PGA (g)	PGV (m/s)	I_a (m/s)	T_d (s)	$a@T_{res,degr}$* (m/s^2)	I_d** (m/s)
nga753	0.64	0.28	3.24	13.89	5.52	1.237
nga779	0.96	1.09	8.37	17.37	15.79	2.241
nga802	0.30	0.27	1.45	15.42	4.61	1.706
nga982	0.57	0.42	3.24	13.98	6.19	0.780
nga1012	0.26	0.27	0.98	12.11	4.02	0.013
nga1085	0.83	0.43	4.50	17.06	15.09	8.255
nga1086	0.60	0.49	2.61	15.10	11.78	4.126
nga3474	0.62	0.31	2.91	9.59	2.41	0.663
sim0001	0.25	0.40	1.25	33.10	3.58	0.625

* $a@T_{res,degr}$ is the spectral acceleration at a degraded resonant period equal to 1.5 times the initial fundamental period of the slope

** I_d is the directionality index as defined in equation (6)

Constitutive Model

A critical state elasto-plastic constitutive soil model was used to accurately simulate the stress-strain behavior of sand during cyclic mobility events (Dafalias and Manzari, 2004). This model predicts reasonably well both the elemental monotonic and cyclic behavior of sand. The model is able to capture the effects of void ratio, and stress state on the mechanical response of sand. It is also able to simulate reasonably the shear-induced volumetric plasticity, and effects of dilation during loading on subsequent unloading paths.

Table 2 Parameters used to model each layer

Layer	**Saturated Unit Weight (Mgr/m^3)**	**Hydraulic Conductivity (m/s)**	**Main Model Parameters**		
Dafalias Manzari Model					
			Calibration Material	**Voids ratio**	
Hydraulic Fill	1.85	3E-3	Toyoura Sand	0.825	
Sand Fill	2.05	3E-3	Toyoura Sand	0.635	
Facing Stone	1.85	3E-2	Toyoura Sand	0.673	
Visco Elastic Model					
			E (kPa)	**V**	**ξ (%)**
Stiff Clay	1.75	3E-7	282400kPa	0.412	10
Sea Water	1.00	-	0.2999999955555 6kPa	0.4999999777 7778	10

The facing-stone properties were assumed to be mechanically similar to dense Toyoura sand, while its permeability is much higher, and its unit weight similar to a loose sand (due to the large voids between the stones). The underlying clay and water are represented as viscoelastic materials.

Sand Model properties

The model properties have been calibrated by Dafalias and Manzari (2004) for Toyoura sand. This calibration has been used for the numerical simulations since the experimental datasets for Toyoura sand provide an excellent basis for calibration of numerical models. The model properties can be seen in Table 3.

Table 3. Dafalias & Manzari Constitutive Model Constants

Constant	Variable	Value	Constant	Variable	Value
Elasticity	G_0	125	Yield Surface	M	0.01
	N	0.05	Plastic Modulus	h_0	7.05
Critical State	M	1.25		c_h	0.968
	c	0.712		n^b	1.1
	λ_c	0.019	Dilatancy	A_0	0.704
	e_0	0.934		n^d	3.5
	ξ	0.7	Fabric-dilatancy tensor	z_{max}	4
				c_z	600

RESULTS

The results are described in four sections. In the first section, damage is associated with earthquake intensity measures. The second section discusses some commonly used analytical correlations. The third section discusses soil behavior during cyclic mobility events by relating damage with excess pore pressure developed in the soil. The fourth section discusses the effect of the directionality of the earthquake motion in designing a slope against seismic damage.

Ground Motion Characteristics

Many correlations of slope damage with ground motion characteristics have been proposed in the literature. Recent work by Travazarou and Bray (2003) was based on an advanced form of a stick-slip deformable Newmark sliding block analysis (Rathje & Bray, 2000) to numerically simulate the stability of a slope. Due to the elastoplastic nature of the problem, characteristics that involve elastic assumptions such as resonant frequency are not successful in quantifying damage.

The damage measure of choice in this research is the average shear strain along the slope has been selected (γ_{ave}), as a damage measure, according to equation (3):

$$\gamma_{ave} = \frac{u(y = H, t)}{H} \tag{3}$$

where u(y=H, t) is the horizontal displacement at the top of the slope at any given time t, and H is the height of the slope.

This measure was also chosen since the final deformation on the top of the slope is crucial for the behavior of structures on top of the slope and because strains in the soil layer affect the lateral pressures on piles.

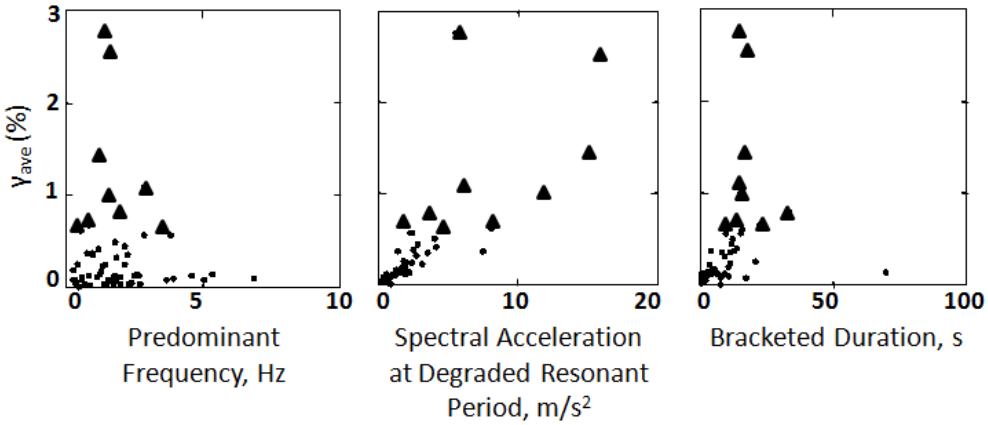

Figure 2. Correlation of predominant frequency, spectral acceleration at the degraded resonant frequency, and bracketed duration with damage; triangles indicate motions that cause large damage

Very popular intensity measures are the predominant frequency of the ground motion, the spectral acceleration at a degraded slope resonant frequency, or the bracketed duration (defined as the time between the first and the last occurrence of an acceleration spike greater than 0.05g). Their correlation with average slope damage is shown in Figure 2. Predominant frequency does not provide a reliable correlation due the elasto-plastic nature of the problem. Also, the greater damage observed close to the 2Hz region is due to the fact that most of the high amplitude motions are observed in this region and not due to resonance. Spectral acceleration at a degraded resonant slope frequency is a reasonable correlation due to the fact that it includes the effects of PGA. Bracketed duration correlates reasonably with damage, because the longer and earthquake the more likely for the slope to liquefy, and also because a larger duration means also most likely greater measured PGA.

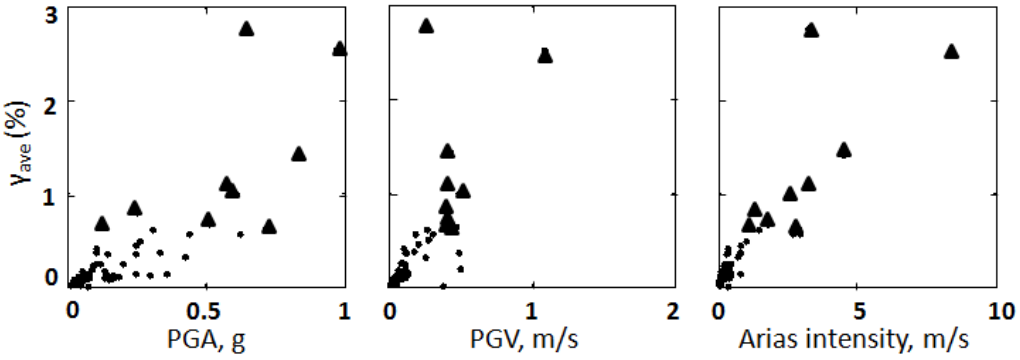

Figure 3. Correlation of peak ground acceleration(PGA), peak ground velocity (PGV), and Arias intensity with damage; triangles indicate motions that cause large damage

Peak ground acceleration (PGA), peak ground velocity (PGV), and Arias intensity are also measures used quite widely. As seen in Figure 3 PGA correlates relatively well with γ_{ave}. This is true since PGA not only includes a measure of the maximum shear forces that excited the slope but also a measure of the duration of the earthquake since longer natural excitations are usually stronger too. PGV does not correlate so well possibly because is smoothes out some acceleration spikes that are important for the accumulation of excess pore pressure and thus important for the seismic stability of the slope. The best earthquake intensity measure has been found to correlate well with slope damage is the Arias intensity, defined by:

$$I_\alpha = \frac{\pi}{2g}\int_0^\infty [a(t)]^2 dt \qquad (4)$$

where g is the acceleration of gravity, and a(t) the recorded acceleration of the motion at time t

The Arias intensity includes the effect of acceleration, duration, and form of the recorded acceleration and thus provides the best measure. It is recommended that for risk assessment of a slope stability risk is associated with Arias intensity on the contrary to the very unrealistic and commonly used magnitude, M.

Analytical Damage Correlations

Analytical solutions that correlate earthquake intensity measures with slope damage are based mostly on sliding bock analyses. Thus, they are very sensitive to the actual value of the yield acceleration used in this analysis. Also, they depend a lot on the actual form of the acceleration. Very similar pulses can produce significantly different predicted slope displacements (Kramer, 1996).

Two very common analytical methodologies have been used; the method of Jibson (Jibson, 1994) that links permanent displacement of a slope with Arias intensity and yield acceleration of a slope, and the method of Bray (Bray J. D., 2007), that correlates permanent displacement on the top of the slope with Arias intensity, yield acceleration of a slope, spectral acceleration at the degraded resonant frequency of a slope, and with the earthquake magnitude. The yield acceleration of the slope (a_y=0.13g) was estimated by performing a pseudostatic analysis with Plaxis.

In Figure 4 we compare both of these analytical solutions with the simulated data. Neither approach shows good agreement with the numerically computed ground deformations. However, the approach of Bray gives a modest improvement on the method of Jibson. These solutions have been created with assumptions more appropriate for drained slopes and hence underestimate the displacement on top of the slope as they do not capture the deterioration of the material due to cyclic shearing under partial drainage conditions. Of course these differences are also attributed to the huge complexity of the seismic slope stability problem.

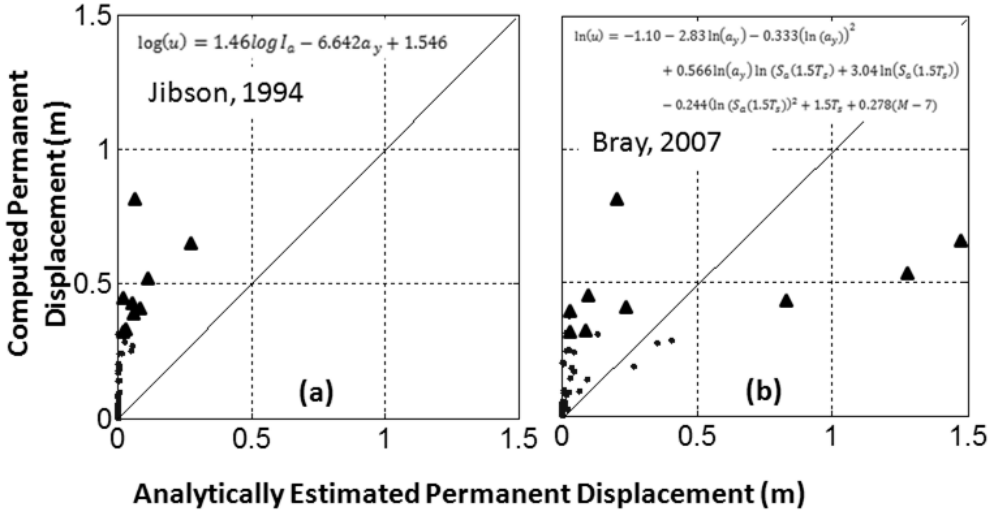

Figure 4 Comparison of the displacement on top of the slope (y-axis) with slope displacements from analytical correlations (x-axis), triangles indicate motions that cause large damage; (a) Jibson (1994) (b) Bray (2007)

Soil Behavior: Excess pore pressure development and associated damage

It is very important to try to associate simulated damage with simulated soil behavior. In order to understand liquefaction damage in the simulated slope we plot in Figure 5 the contours of the final

deformed states from the 9 more "damaging" ground motions, in the analyzed suite of ground motions. Displacements along the slope can be as high as one meter, but complete instability is not predicted in any case. It can be seen that strains are mostly uniform inside the slope. As the simulations did not generate very well-defined shear planes, it is more logical to use the average shear strain over the height of the slope as a measure of damage.

Figure 6 summarizes the simulated excess pore pressure ratios ($\Delta u/\Delta\sigma'_{v,0}$) at the end of the strong ground motion. The end of the strong ground motion is defined as the last occurrence of a spike larger or equal to a=0.05g. The excess pore pressures are largest at location behind the slope. Closer to the slope itself the downslope shear strain causes large dilative strains during the earthquake excitation (and these elements approach critical state shear conditions). This zone of dilation (i.e. with negative shear-induced pore pressures) can be clearly seen as a zone of lower excess pore pressures beneath the crest of the slope.

Since we are dealing with saturated slopes, we can assume that if no excess pore pressure ratio is developed then no strains develop in the slope. Also, if the excess pore pressure ratio reaches unity then there is no available shear strength in the model, and the associated strain in the slope will become infinite. All, other states lie in between these two limiting scenarios.

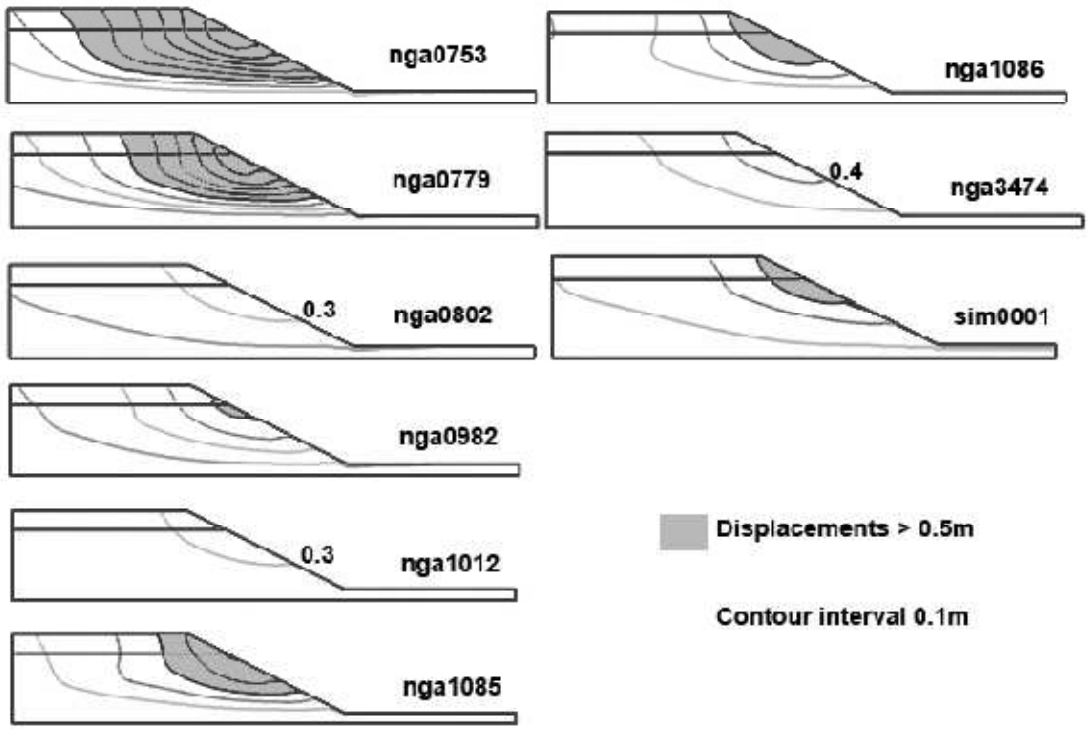

Figure 5. Final deformed shape at end of shaking

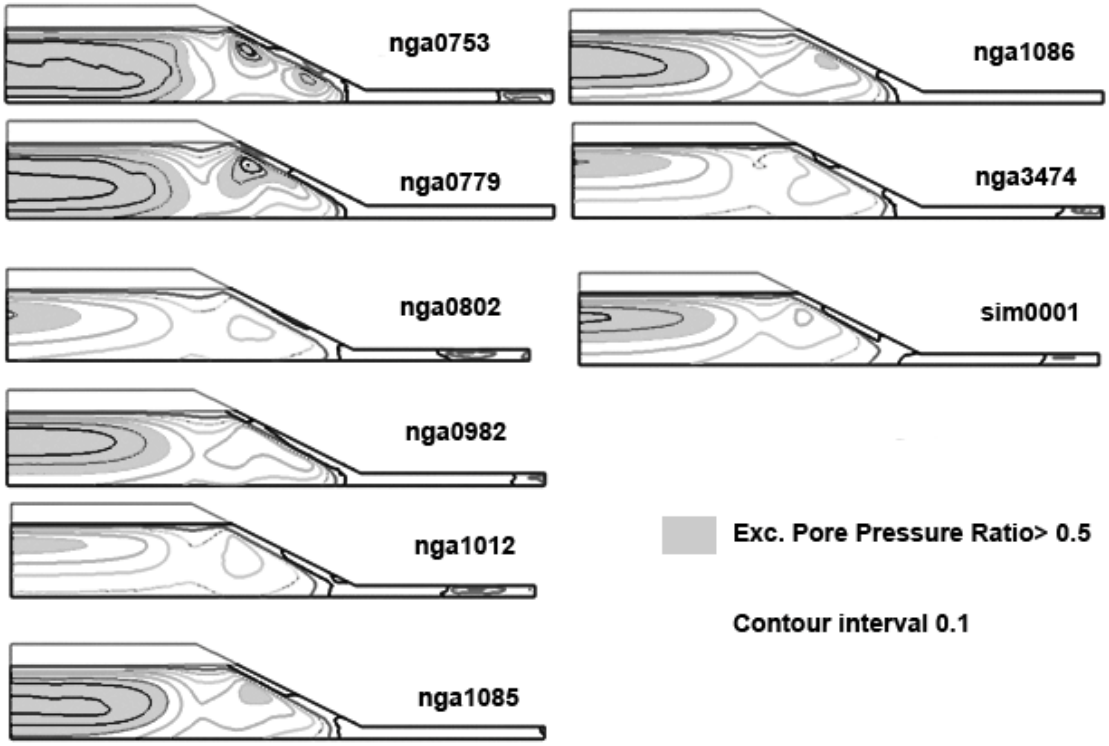

Figure 6. Excess pore pressure ratios at the end of the strong ground motion

For this reason in Figure 6 we correlate the average shear strain developed in the slope at the end of shearing with the average bracketed excess pore pressure ratio developed in a region close to the maximum shear zone according to equation (6):

$$\gamma_{mean} = s_f \cdot \frac{\frac{\Delta p}{\sigma'_{v,0}}}{1 - \frac{\Delta p}{\sigma'_{v,0}}} \tag{5}$$

where s_f is a slope factor that defines the damage resistance of a slope to earthquake induced pore pressures. The average bracketed excess pore pressure ratio is defined as the time average of the excess pore pressure average in a specific region (Region **A** as seen in Figure 1), during the bracketed duration of the motion. In this work bracketed duration is defined as the duration between first and last excedance of an acceleration spike of a=0.05g.

Figure 8a shows that results are very consistent with this correlation. It should be noted that the fact that excitations are from real ground motions improves the correlation since real excitations that have greater intensity, they also have more cycles, leading to both pore pressure accumulation and shear damage. The actual region in which we average the bracketed excess pore pressure ratios is not very critical in this procedure.

These results have some very important implications in designing against liquefaction in a slope. Rather than performing a large series of dynamic analyses for different ground motions (to get a complete picture of damage in a given slope), an engineer could sample his dataset to consider only 3-4 motions with varying Arias Intensities (thus different damage states). From there it would be possible to estimate the

slope factor s_f. Then for a given design damage one can estimate the expected excess pore pressure in the given slope and design drainage liquefaction mitigation systems.

These analyses are also used to evaluate possible pile damage. In order for this to be accomplished the output of the free field analyses is provided as input to macro-elements that simulate the soil pile interface (Varun and Assimaki, 2008). In Figure 7 we see the final predicted horizontal displacements of the soil in the free field analyses along two sections where piles are installed. Soil movement produces significant bending, and causes one or two points of deflection in the piles. Since the magnitude of differential displacements from the top to the bottom of the piles is similar in both locations, we can expect more damage on the shorter pile than the larger one. If the piles are well embedded in the underlying Bay mud layer then we should expect much more significant damage due to the downslope ground movements.

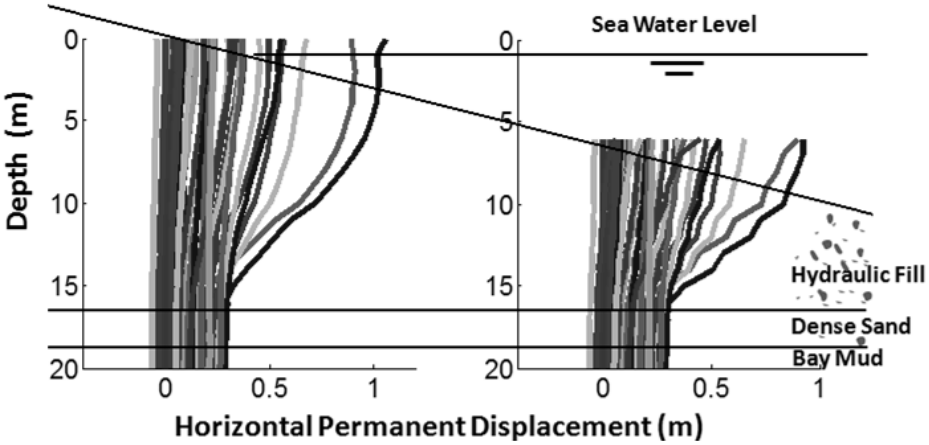

Figure 7 Final horizontal displacements along two sections where piles are installed for all the ground motions. Each line represents the final horizontal deformation profile for each motion

Directionality Effects

When analyzing a suite of motions for design purposes, it is important to decide if the direction of the used excitation is important. For example, a designer might be concerned whether the left hand side and the right hand side of an embankement beneath a highway are going to develop similar damage for similar dynamic excitation.

At first a directionality measure is established. Since Arias intensity provides the best measure of intensity we consider a directionality index I_d defined by subtracting the Arias intensity of only the negative side of the excitation from the Arias intensity of the positive side of the excitation. This is defined as the directionality index of the ground motion, a measure of how directional an excitation is.

$$I_d = \frac{\pi}{2g}\int_0^{\infty}[< a(t) >]^2 dt - \frac{\pi}{2g}\int_0^{\infty}[< -a(t) >]^2 dt \qquad (6)$$

where <x>=x for x>0, and <x>=0 for x<0

We divide our samples into two datasets; a suite of excitations that drive the slope mostly downslope and to a suite of motions that drive the slope mostly upslope. In this particular example negative values of I_d are associated with net downslope accelerations and positive values of I_d are associated with net upslope accelerations. Next, since we found out that the correlation between the average shear strain and average

excess pore pressure ratio is very good, we estimate this correlation for the two datasets separately and for the two datasets simultaneously.

If the directionality effects are important then the correlation coefficient in the separate datasets should be better that the correlation coefficients for the combined set of ground accelerations. Figures 8a, b, and c show that this is not the case and similar correlations are obtained for all datasets. Also, we would expect that motions driving the slope mostly downslope to have a slightly larger slope factor, s_f. Although, this is the case the margin is so small that we can assume the effect is negligible. Thus, directionality of the excitation motions appears to have little effects on damage in the slope.

Figures 9a, b, and c consider the directionality issue in more detail by comparing the average slope shear strains for the 3 ground motions with the highest absolute directionality index (I_d, Table 1) that are applied in the downslope and upslope directions. The results show minimal differences in computed shear strains for nga0779 (I_d = 2.24 m/s, Fig. 9a) but larger differences for nga1085 and nga1086 (I_d = 8.26, 4.13 m/s, respectively; Figs. 9b, c). These results suggest that directionality is only a significant issue if I_d > 3-4 m/s.

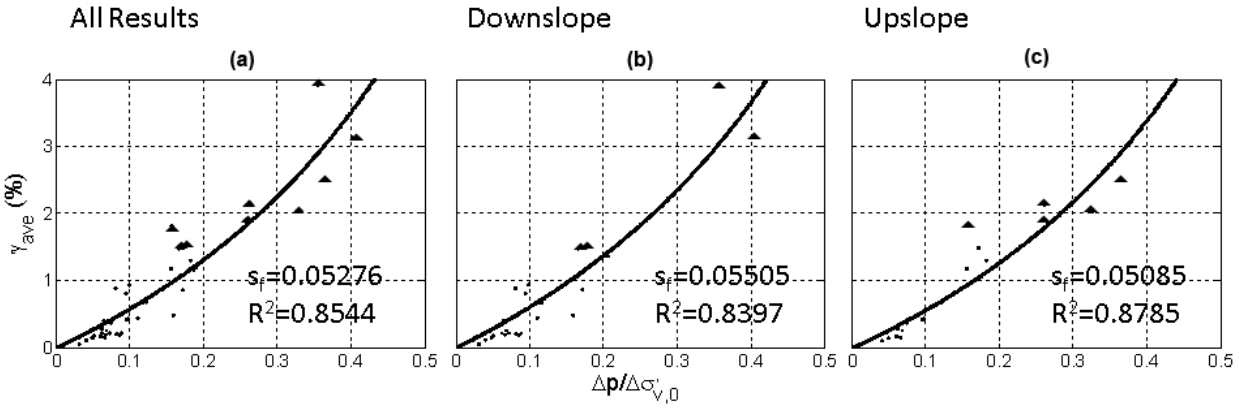

Figure 8. Estimation of the effect of directionality in the simulated ground motions

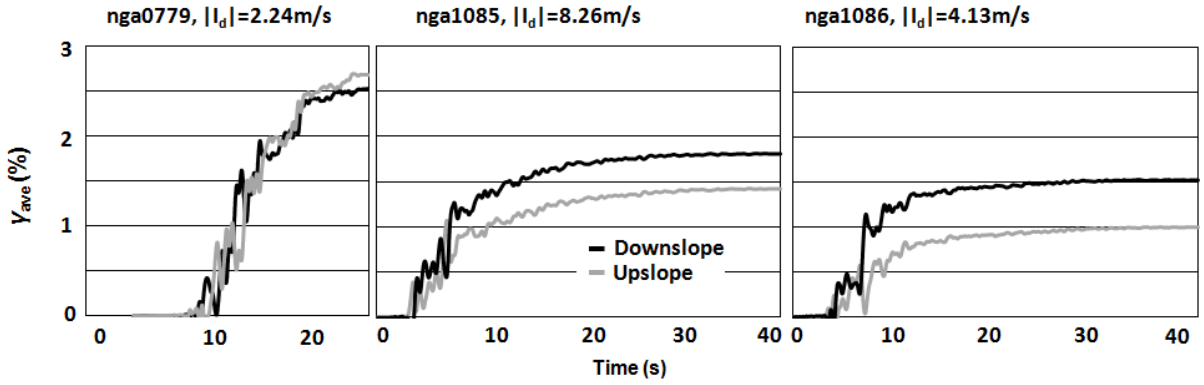

Figure 9. Damage observed in the slope for the three more directional seismic motions before and after we invert the motion direction

CONCLUSIONS

This paper has shown that Arias intensity correlates very well with numerical simulations of slope damage, defined using an average slope shear strain, due to seismic ground motions. It has also been shown that accumulation of excess pore pressure correlates very well with associated damage (Figure 8). It is possible to assess the directionality of a ground motion through a directionality index inspired by Arias intensity. This index is able to distinguish cases where directionality can have a significant impact on the response of the slope.

AKNOWLEDGEMENTS

The authors would like to acknowledge support from NSF grant No. CMS-0530478, under the project NEESR Grand Challenge, "Seismic Risk Management for Port Systems". They would like to acknowledge use of cluster computer resources available through the SMART Center for Environmental Sensing and Modeling (CENSAM). Antonios Vytiniotis would also like to acknowledge support from the Alexander S. Onassis Public Benefit Foundation.

REFERENCES

Assimaki, D. (2004). *Topography effects in the 1999 Athens earthquake: Engineering issues in seismology.* Cambridge.

Bray, J. D. (2007). Simplified Seismic Slope Displacement Procedure. *Earthquake Geotechnical Engineering* (pp. 327-353). Thessaloniki: Springer.

Bray, J., & Travasarou, T. (2007). Simplified procedure for estimating earthquake induced deviatoric slope displacements. *Journal of Geotechnical and Geoenvironmental Engineering* , 381-392.

Chiou, B., Darragh, R., Gregor, N., & Silva, W. (2008). NGA Project Strong-Motion Database. *Earthquake Spectra* , 23-44.

Dafalias, Y. F., & Manzani, M. T. (2004). Simple Plasticity Sand Model Accounting for Fabric Change Effects. *Journal of Engineering Mechanics* , 622-634.

Jeremic, B. (2008). *Lecture Notes on Computational Geomechanics: Inelastic Finite Elements for Pressure Sensitive Materials.* Department of Civil and Environmental Engineering, University of California, Davis.

Jibson, R. (1994). Predicting earthquake-induced landslide displacements using Newmark's sliding block analysis. *Transportation Research Record 1441* , 9-17.

Kramer, S. L. (1996). *Geotechnical Earthquake Engineering.* Upper Saddle River: Prentice-Hall, Inc.

Makdisi F, S. H. (1978). Simplified procedure for estimating dam and embankment earthquake-induced deformations. *Journal of Geotechnical Engineering* , 849-867.

Mazzoni, S., McKenna, F., & Fenves, G. L. (2005). *Opensees Command Language Manual.*

Newmark, N. (1965). Effects of earthquakes on dams and embankments. *Geotechnique* , 139-160.

Rathje, E., & Bray, J. (2000). Nonlinear coupled seismic sliding block analysis of earth structures. *Journal of Geotechnical and Geoenvironmental Engineering* , 1002-1014.

Travazarou, T., & JD, B. (2003a). Optimal ground motion intensity measures for assessment of seismic slope displacements. *Pacific Conference on Earthquake Engineering.* Chirstchurch, New Zealand.

Varun, & Assimaki, D. (2008). A nonlinear dynamic macroelement for soil-structure interaction analyses of pile-supported wharfs. *Proc. 4th Decennial Geotechnical Earthquake Engineering and Soil Dynamics Conference (GEESD).* Sacramento, CA.

Vytiniotis, A. (2009). *Numerical Simulation of the Response of Sandy Soils Treated with Pre-fabricated Vertical Drains.* Cambridge.

Zienkiewicz, O., & Bettess, P. (1978). Fluid-structure dynamic interaction and wave forces. An introduction to numerical treatment. *International Journal for Numerical methods in Engineering* , 1-16.